(Online) ISSN 2712-0562
Sustainable Engineering and Innovation
Original Research
Vol. 7, No. 2, 2025, pp.537-558
https://doi.org/10.37868/sei.v7i2.id464

Engineering a low-cost, expendable fixed-wing drone for search and rescue missions using readily available components

Michael Ray D. Maligro[1*], Donato L. Juayang Jr.[2], Alan Pierre-Miguel R. Gultia[3], Paula Alexandra B. Padro[4], Ben James T. Cuajotor[5], Michael Caleb P. Obalan[6], Dynah Ruiza V. Opeso[7], Kristy Lailanie G. Ompad[8], Edison U. Montes[9], Sherwin A. Guirnaldo[10], John Carl O. Salaan[11], Noel M. Hernandez[12], and Jonathan C. Maglasang[13]

[1,2,3,4,5,6,7,8,10,11,12] Department of Mechanical Engineering and Technology, Mindanao State University – Iligan Institute of Technology, Philippines

[9,13] Department of Mechanical Engineering and Technology, Cebu Technological University, Philippines

*Corresponding author E-mail: michaelray.maligro0808@g.msuiit.edu.ph

Received Mar. 31, 2025
Revised Aug. 27, 2025
Accepted Sep. 4, 2025
Online Nov. 14, 2025

Abstract

This paper describes the design and aerodynamic performance evaluation of a low-cost, expendable fixed-wing UAV for humanitarian purposes built with off-the-shelf components. The drone is designed for quick deployment in disaster relief, search and rescue, and medical delivery operations. The aerodynamic performance, stability, and flight performance were evaluated using DATCOM, XFLR5, and Computational Fluid Dynamics (CFD) analyses. Results indicate that the wing and fuselage of the UAV are well designed, which significantly enhanced the lift-to-drag ratio, endurance, and efficiency. The employment of commercially available parts allows for cost-effective, scalable, and replicable platforms. The payload can be adapted and, since the drone is modular, it is also versatile. Future work will focus on enhancing structural integrity while maintaining cost efficiency, incorporating vision-based survivor detection for search and rescue operations, and conducting field tests to validate performance under diverse conditions. This study is part of the design effort towards accessible and cost-efficient UAV solutions for humanitarian operations, bridging the gap between affordability and performance.

Keywords: Semi-disposable UAV, Commercial off-the-shelf components, Aerodynamics

1. Introduction

Drones capable of operating in high-risk environments play a critical role in supporting humanitarian operations, particularly search and rescue (SAR) missions. The utilization of unmanned aerial vehicles (UAVs) in search and rescue (SAR) is a significant step forward in performing time-critical and high-risk operations. In contrast to conventional systems, UAVs present unique benefits in mobility, response time, and situational awareness [1][2]. These drones have lightweight, advanced sensors and modular payloads to assist them in mapping disaster zones, searching for survivors, and ensuring aid gets on the scene as fast as possible. One example of such an application is depicted in Figure 1, where a drone is employed to scan a collapsed open-pit mine.

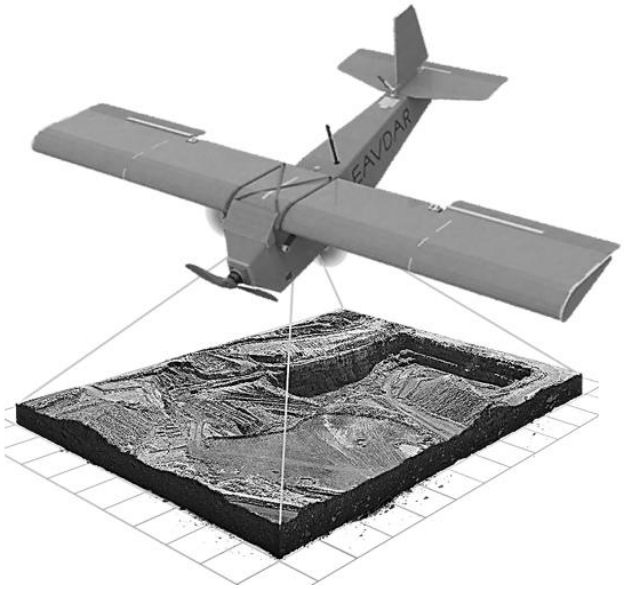

Figure 1. Drone mapping for SAR through computer vision

Despite their advantages, the practical use of UAVs in SAR operations is relatively limited due to cost. High-end commercial drones equipped with advanced features are also prohibitively expensive, making them unaffordable for the majority of organizations, particularly research and education sectors [3]. To address such demands, low-cost UAVs based on open-source designs with readily available materials have gained popularity. This method emphasizes designing the most effective and low-cost SAR drones to achieve primary SAR missions, even at a loss of a few advanced abilities. Within this context comes the concept of disposable drones—those built with readily available materials that can be used once or a few times. Though still in the early stages of adoption, this technology is gaining attention for its potential to make a real impact. One example is a drone developed by SYPAQ [4] as seen in Figure 2.

Figure 2. Cardboard drone by SYPAQ [4]

With the use of drones as a disposable platform comes ethical and practical considerations, especially when mission success overrides consideration of the drone. Key considerations encompass responsibility for deployment, the safety of civilians, potential environmental consequences, and the danger of misuse in unauthorized or ethically dubious actions [5]. These issues are particularly acute in high-risk situations, such as SAR operation scenes, where some degree of loss could be substantial. Careers in addressing these challenges

will have to strike this balance between operational effectiveness on the one hand and responsible, risk-aware use of technology on the other. To fully benefit from the potential of UAVs in these areas, close cooperation between researchers, manufacturers, and policymakers is required.

Creating low-cost, easy-to-build drones requires out-of-the-box thinking—including the use of cheaper materials, modular construction methods, and the latest in 3D printing. These methods could make drones far more accessible and scalable. UAV technology has the potential to mature from a niche technology into an indispensable tool for the most diverse applications, including SAR operations, and beyond that for general humanitarian use if these obstacles were to be addressed. To address these requirements, the drone design proposed in this paper is described, with the objective of offering an inexpensive, disposable cost platform specifically tailored to the requirements of SAR missions.

The semi-disposable UAV, called Expendable Aerial Vehicle for Disaster Area Response (EAVDAR), is built from off-the-shelf components, making it cheap and simple to manufacture. The isometric view of the computer-aided EAVDAR design is presented in Figure 3. Designed to support important missions including surveillance, delivery of cargo, and emergency response, it has a modular interchangeable design and can be easily adapted to different SAR situations, and deliver survival kits, tailored for varying requirements in the field. The EAVDAR is a low-cost, easy-to-construct, and portable system that can be put in place, utilized, and, if required, destroyed with minimal financial loss. In this paper, we address three main aspects: design, payload system, and flight dynamics performance. This new development will be broken down into the design and manufacturing processes, as well as the aerodynamic performance, to show that this cutting-edge solution is real.

Figure 3. Isometric view of EAVDAR

2. Design

The EAVDAR has simplicity in design and functionality. The airframe is constructed from foam board and 3D-printed plastics for cost efficiency while preserving structural integrity. To improve the low cost and ease of construction, the present design uses commercially available off-the-shelf components like a flight controller and communication systems. EAVDAR is specifically designed for search and rescue operations and has a versatile design to accommodate a variety of payloads and recover people in different environments. Such versatility facilitates rapid reconfiguration to new mission needs, thereby maximizing the overall usage and efficiency of the system. Moreover, its semi-disposable nature makes it highly suited for operation in higher-risk zones where loss is more prevalent. This type of design makes sure that the device will be usable during emergency response missions, minimizes the device's potential cost, and alleviates probable economic impact.

2.1. General specifications and design features

The following sections discuss the specific core attributes, such as dimensions, internal volume, propulsion, battery systems, avionics for reliable control and communication, and payload capabilities of EAVDAR. The unique features of these models underscore their adaptability to various operational needs, offering a thorough understanding of their design and integration across different environments.

2.1.1. Dimensions and volume

EAVDAR is a fixed-wing UAV designed with a maximum takeoff weight of approximately 13 kg, which has a complementary advantage between versatility and maneuverability. The airframe is made from lightweight foam board, while a brace of aluminum rods and carbon bracing adds strength and rigidity. Another characteristic of the design is the high-wing, providing better stability and control, especially advantageous in humanitarian operations where low-speed flight is involved. The main wing uses a NACA 4415 [6] airfoil profile, which is well-suited for stable flight and maneuverability because of high lift and low drag. With a wingspan of 2 meters and a chord length of 30.7 cm, the design provides sufficient lift and stability that are completely reliable for long loitering and accurate flight control. The overall dimension of EAVDAR is presented in Figure 4.

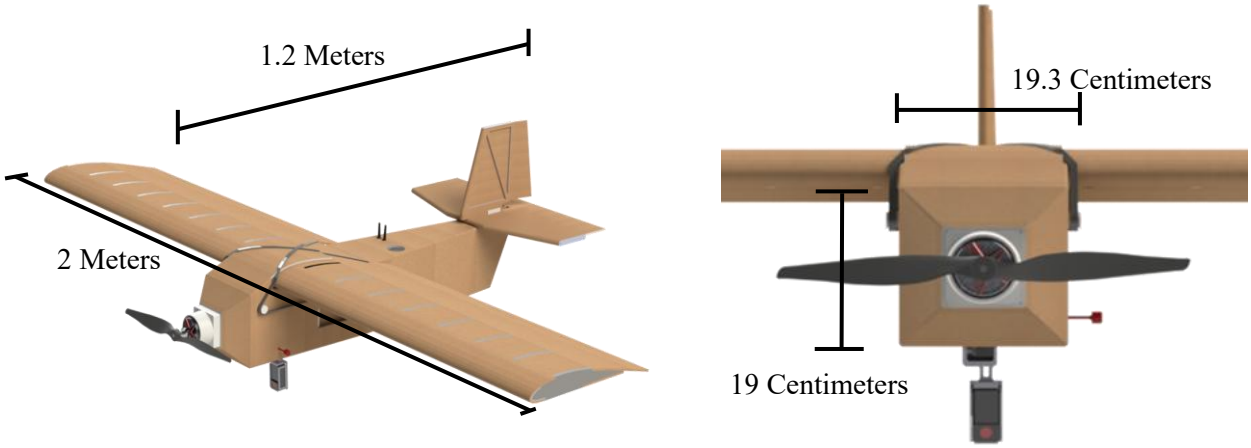

Figure 4. General dimensions of EAVDAR

The drone has a fuselage designed as a rectangular box measuring 19 cm x 19.3 cm x 39.5 cm, tapering into a 62 cm tail, bringing the total drone length to around 120 cm. This design maximizes internal space while maintaining aerodynamic efficiency. The internal volume of roughly 18 liters accommodates avionics, the battery, and payloads in the most efficient manner. Horizontal and vertical stabilizers having an area of 350 cm² per semi-span are important for flight stability and control, which is necessary due to the mission in humanitarian operations. Figure 5 shows the different profiles of EAVDAR and presents its overall structure and design.

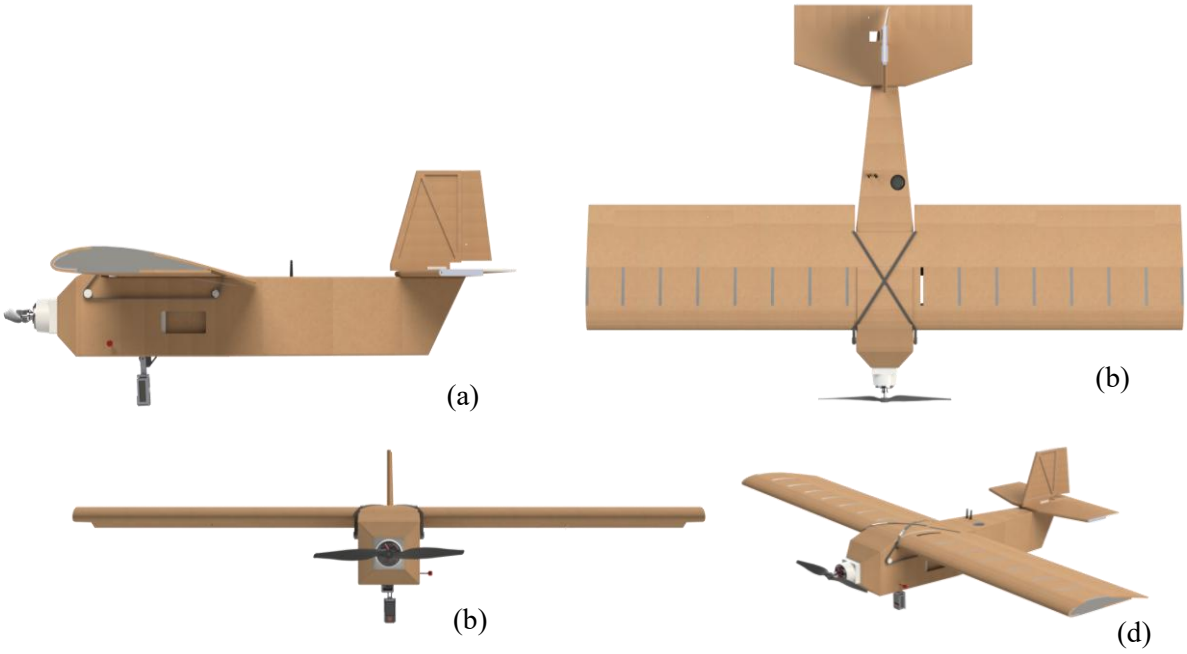

Figure 5. (a) Top, (b) side, (c) front, and (d) isometric views of EAVDAR

2.1.2. Internal structure

Complementing its aerodynamic design, the propulsion system of EAVDAR is carefully designed between performance and dependability. Intelligently placed within the structure of the drone and embedded within the aircraft system, it helps to ensure optimal performance throughout. As can be seen from Figure 6, the system adopts a 16-inch front-mounted propeller, with a BLDC (Brushless DC) motor, able to produce 10 kg of thrust. The puller or tractor configuration was chosen as an efficient layout with the ability to convert battery power into thrust, important for fairly long-duration flights needed for humanitarian missions [7]. However, this is at the expense of creating some turbulence over the aircraft's body [8]. The drone is powered by a 22.2-V battery pack of 10 amp-hour to 30 amp-hour for maneuverability and endurance in various mission requirements. A 10 amp-hour battery for short missions (approximately 30 km) and a 30 amp-hour battery for extended missions (approximately 120 km). The drone operates at a cruise speed of 85 kph, which strikes a good balance between efficiency and quick deployment, allowing it to cover a large area without draining the battery. With an empty weight of 5 kg, the drone can handle a payload of 8 kg, which can carry mission-critical supplies and equipment for added flexibility in a range of operational scenarios.

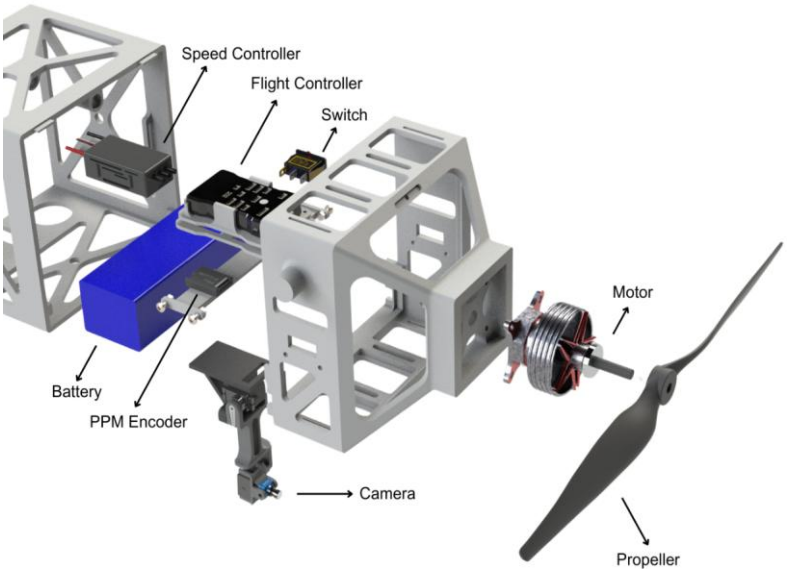

Figure 6. Propulsion and electrical system of EAVDAR

2.1.3. The avionics system

The avionics system of the EAVDAR is to match its propulsion and structural elements, ensuring good control and predictable behavior are achieved in order to maintain overall efficiency. By using commercial off-the-shelf components in a custom 3D-printed support frame, the system achieves both ease of maintenance and adaptability to various missions. Additionally, the strategic placement of antennas optimizes signal reception and transmission— an essential aspect during long-range operations to maintain communication. The telemetry system, as shown in Figure 7, works within the 915-928 MHz range and is capable of being downlinked at a range of 40 km, which is important for stretched mission scenarios.

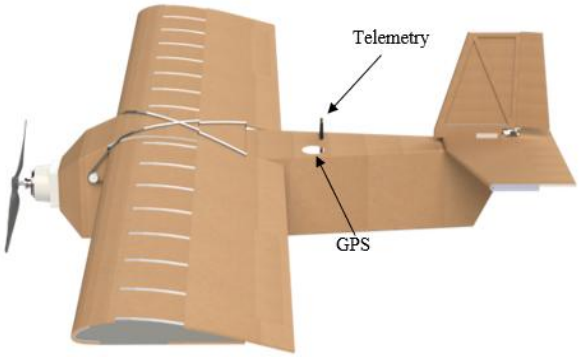

Figure 7. EAVDAR telemetry system

Central to the avionics is a commercially available autopilot system (e.g. Pixhawk 2.4.8), which also allows to perform autonomous navigation and flight control. This feature greatly contributes to optimizing the mission by featuring pre-programmed flight paths and real-time adjustments. To ensure secure operation, a strong fail-safe system enables the drone to either return to a designated home point or execute a safe landing in case of communication loss or system failure. Table 1 presents a summary of the specifications and features of the avionics system.

Table 1. Avionic system details

Specification/Feature	Details
Component Materials and Sourcing	Commercial off-the-shelf components, 3D-printed support frame and rack, strategic antenna placement
Home-to-UAV Telemetry Frequency	915-928 MHz up to 40km
Support for LoRa Portable RC Controller	Yes (ELRS/CRSF)
Support for Autopilot System	Yes
Dedicated Flight Computer	Capable
Fail-Safe Systems	Yes
Base Station and Tracker System	Yes (Enables long-range FPV: > 30km)
Encrypted Operation	Yes (AES)

For long-range first-person view (FPV) operations, the base station and tracker system support long ranges beyond 30 km, delivering real-time video and telemetry for command and feedback. In order to protect communications from being intercepted during high-risk missions, AES (Advanced Encryption Standard) encryption is used to protect, particularly, the transmission of data and mission information.

2.1.4. External structure

The external structure of EAVDAR is made out of foam board for simplicity of construction and compatibility with off-the-shelf materials. This material was selected for its lightweight properties and its ability to protect the drone's internal components. The manufacturing process starts with fine laser cutting, which creates the cutouts and crease lines. The creases enable accurate folding along designated sections for a precise and easy assembly. Figure 8 shows the cutout sections for the nose, body, and rear of the EAVDAR.

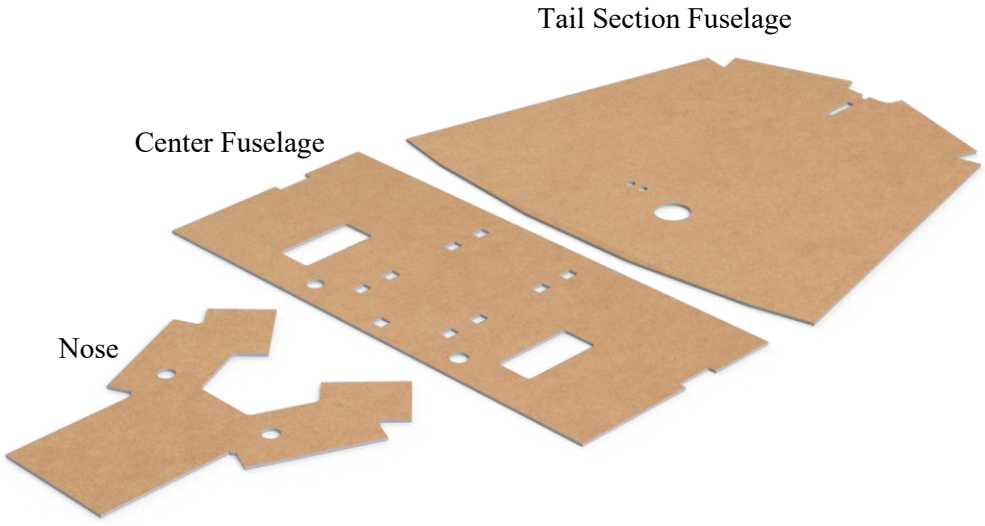

Figure 8. Foam board cutouts of the fuselage

Once the laser-cutting is finished, the external structure is waxed for increased water resistance. This protective layer provides an added safety for the drone, ensuring it can withstand wet conditions during flight.

2.1.5. EAVDAR specifications and features

The drone is premeditated for humanitarian efforts, revealing state-of-the-art skill central to search, surveillance, and relief efforts. Equipped with imaging capabilities, it has search capabilities and real-time surveillance, and can provide instant asset management in any emergency. Its multi-vision system consists of color, night, LiDAR, and thermal imaging technologies, allowing it to operate in numerous environmental conditions. Table 2 outlines the summary of EAVDAR's specifications.

The drone can also operate effectively in a GPS-denied environment utilizing inertial navigation systems, which is an absolute necessity for missions where GPS is degraded or unavailable. Cost efficiency remains the central aspect of the design, utilizing low-cost materials and systems that are energy-saving and conducive to economic sustainability without sacrificing performance. Practical design, which includes an open hatch to have access and maintenance, and a folded camera as shown in Figure 9, enables the platform to be more operationally useful. Additionally, a configurable payload enhances its versatility, allowing the drone to meet a wide range of mission profiles. Table 3 outlines the key features integrated into the EAVDAR system.

Table 2. EAVDAR specifications and parameters

Specification/Feature	Details
Model	Expendable Aerial Vehicle for Disaster Assessment and Response
Maximum Takeoff Weight	Approximately 13 kg
Airframe Construction	Lightweight, durable foam board reinforced with Aluminum rods and a 3D printed PETG frame.
Wing Configuration	Straight, unswept, untapered main wing, NACA 4415 profile, 2 meters wingspan, 29 cm chord lengths
Fuselage	Rectangular box shape, 19cm by 19.3 cm by 39.5 cm dimensions, 62 cm tapering tail, 18 liters volume
Stabilizers	Horizontal and vertical stabilizers, 350 cm² area per semi-span
Propulsion System	16-inch front-mounted propeller, 10kg BLDC motor
Battery	22.2-V battery pack (10 amp-hr, upgradable to 30 amp-hr)
Performance	Estimated Range: 30 km (up to 180 km with 30 amp-hr), Cruising Speed: 85 kph
Empty Weight	5 kg (10 Ah Battery)/7 kg (30 Ah Battery)
Payload Capacity	8 kg

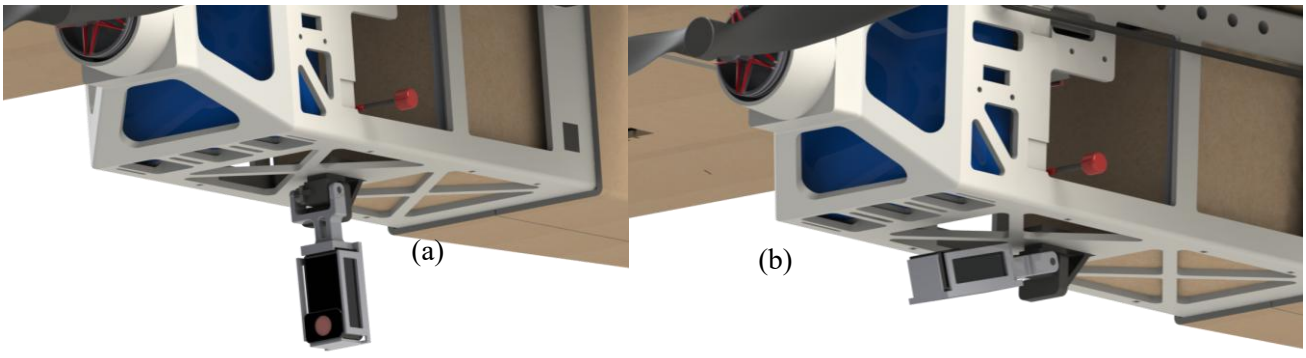

Figure 9. Foldable camera mechanism: (a) open, and (b) closed configuration

Table 3. Notable specific features

Specification/Feature	Details
Full Autonomous AI-Driven Operation	Capable
Multi-Supported Vision System	Yes (Color, Night, Thermal, etc.)
Configurable Payload	Yes (SAR, Relief, Medical)
Support for GPS-Denied Operation	Yes (VS-INS Fusion)
Low-Cost Operation	Yes

Figure 10 presents the relationship between flight range and payload mass for two battery configurations: a 30Ah battery and a 10Ah battery. The range was estimated using a Breguet-type endurance relation adapted for battery-electric propulsion [9]:

$$E_{\text{battery}} = \eta_{\text{elec}}\,\eta_{\text{prop}}\sqrt{\frac{27}{512}\cdot\frac{1}{W/S}\cdot\frac{1}{W^2}\cdot\frac{\rho(\pi Ae)^3}{C_{D0}}}\,U_{\text{bat}}, \quad (1)$$

Where aerodynamic parameters were obtained from a quadratic drag polar fit, $CD = CD0 + KC^2_L$ with $K = 1/(\pi Ae)$, and CD–CL values were derived from CFD simulations. Battery energy was computed as $U_{bat} = V \times Q \times \eta_{discharge}$. Two battery capacities (10 Ah and 30 Ah at nominal voltage) were considered, with an effective propulsion efficiency of 30% to account for battery, motor–controller, and propeller losses [10]. Flight range was then determined as $R = Vcruise \cdot Ebattery$, with cruise speed taken at maximum lift-to-drag ratio. Results show that range decreases with increasing payload for both cases: the 30 Ah battery achieves ~150 km at zero payload and ~75 km at 8 kg payload, while the 10 Ah battery achieves ~70 km at zero payload and <30 km at 8 kg. These results emphasize the trade-off between payload capacity and endurance, with higher-capacity batteries providing significantly improved range performance.

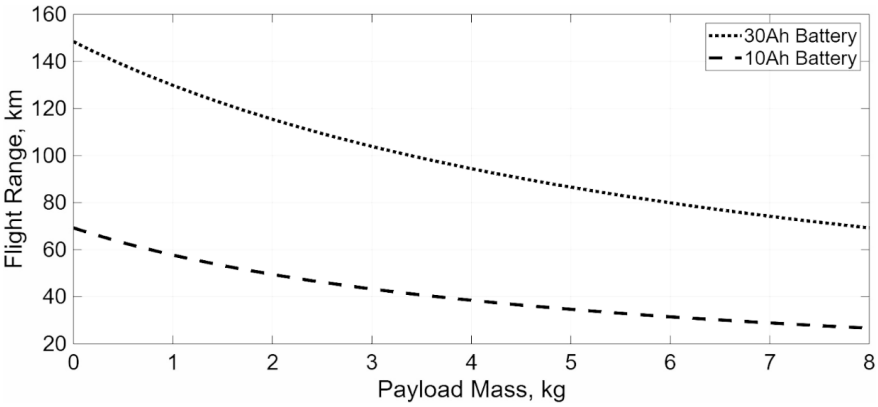

Figure 10. Range performance to payload and battery configuration

2.2. Payload system

The payload system of EAVDAR is designed for a maximum level of versatility, allowing the drone to be equipped with various types of mission-oriented payloads. The system, which has an 18-liter payload volume and 13 kg of total takeoff weight, enables it to carry critical supplies during SAR operations. As shown in Figure 10, the modular payload bay box is constructed from foam board and can be quickly modified to carry relief supplies, medical packages, and specialized equipment to move between multiple mission tasks. Additionally, the system allows the attachment of sensors such as thermal imaging cameras or LiDAR to improve the drone's capacity to locate survivors in challenging environments. This flexibility makes EAVDAR a very powerful tool for search and rescue missions that require the saving of lives beyond that of traditional SAR.

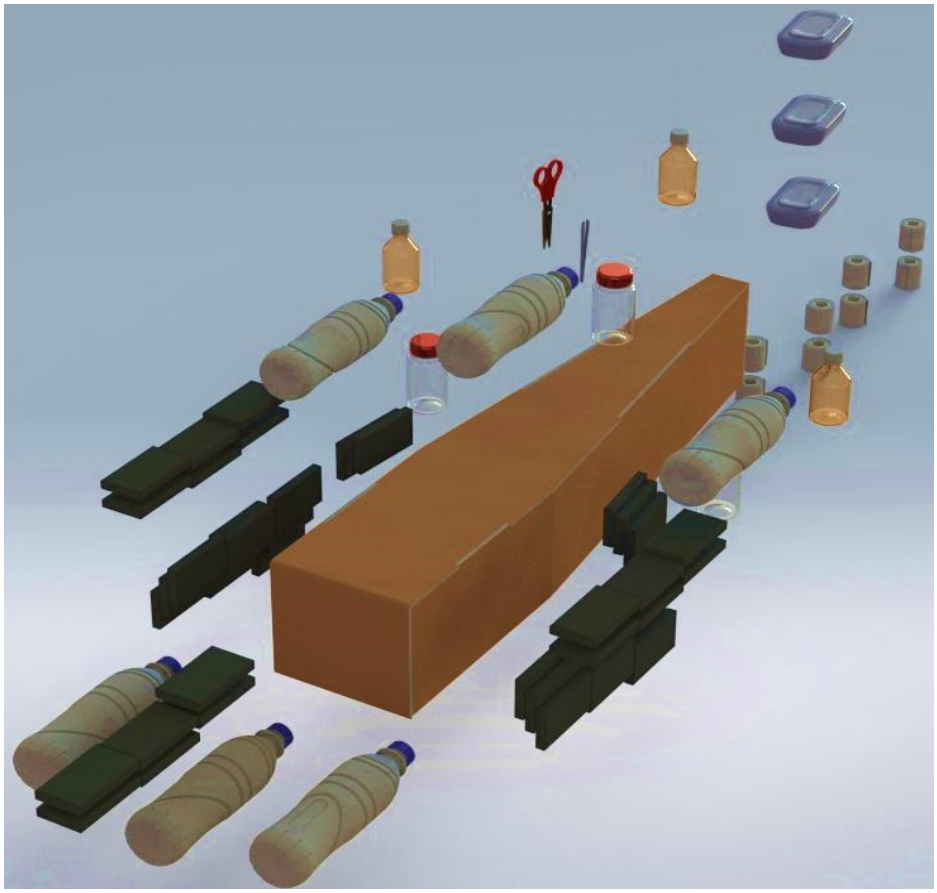

Figure 11. Fuselage survival kit configuration

Capitalizing on its adaptable payload architecture, EAVDAR is designed to be a rapid and efficient means of delivering survival aids to those in distress, such as in disaster and remote locations where conventional multi-rotor drones are restricted by range. The drone can traverse huge and hostile terrain with on-board sensors to find survivors. The pilot will then choose the closest landing location, with no consideration for terrain, as it doesn't have to recover the drone. Survivors will weld a supply box accessed from the tail section upon landing that holds vital survival equipment. As illustrated in Figure 11, the internal storage of EAVDAR securely holds the survival kit box. Along with the supplies, a written note will instruct survivors to ensure the safety of the main fuselage, as it contains important avionics that can be reused, while the foam board skin and wings can be discarded. This method widens the scope of life-saving assistance, brings environmental benefits by enabling valuable electronic components to be recovered for future missions, and increases resource efficiency.

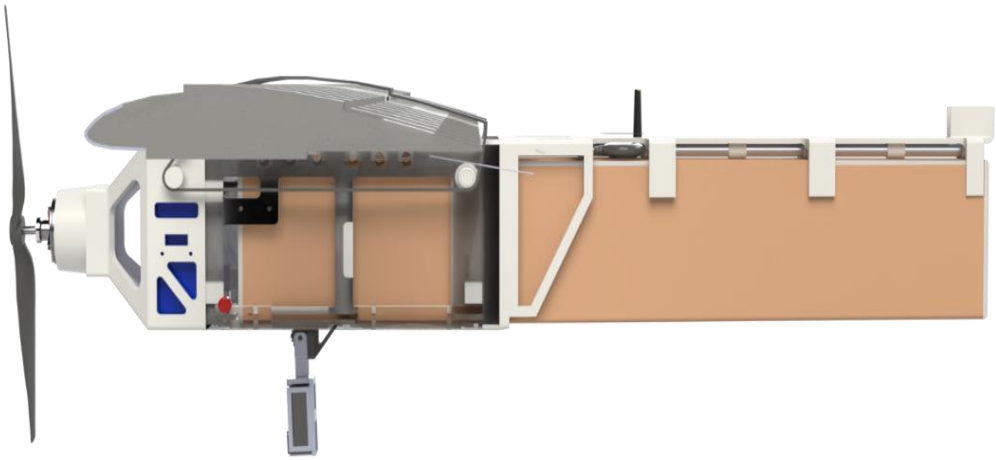

Figure 12. EAVDAR with the survival kit box

2.3. Configurable wing system

2.3.1. Wing design and assembly process

EAVDAR's wing system is engineered for rapid assembly, field deployment, and mass production, making it well-suited for missions that demand quick setup. The wings are constructed using ultra-lightweight foam boards, providing an ideal compromise between strength and production cost-effectiveness. Foam board panels are easy to cut and crease to pre-defined guide profiles, making it easy to produce the UAV without the use of specially fitted tools and a more complicated assembly. This design approach allows the UAV to be assembled, repaired, or converted with minimal means.

The wing is reinforced by an aluminum spar that adds structural support without adding much weight, thus increasing rigidity and enabling greater flexibility in wing design. Internal reinforcement reduces excessive flexing in flight and ensures accurate distribution of loads in terms of aerodynamic loads. The modular mounting system enables quick detachment and reattachment of the wing sections from the fuselage, thus increasing operations like transportation, storage, and replacement. Figure 12 illustrates folding the wing system.

The simple assembly method of EAVDAR exhibits excellent flexibility and is suitable for diverse working conditions. In cases where a wing section is damaged or where the mission dictates a modified wing section to achieve an alternative aerodynamic profile, a replacement can be quickly fabricated and installed, restoring the UAV's flight capability within a minimum time. This modular design approach ensures that EAVDAR maintains an operationally practical, cost-effective airframe, particularly advantageous for rapidly reconfiguring air systems that require frequent redeployment and field maintenance.

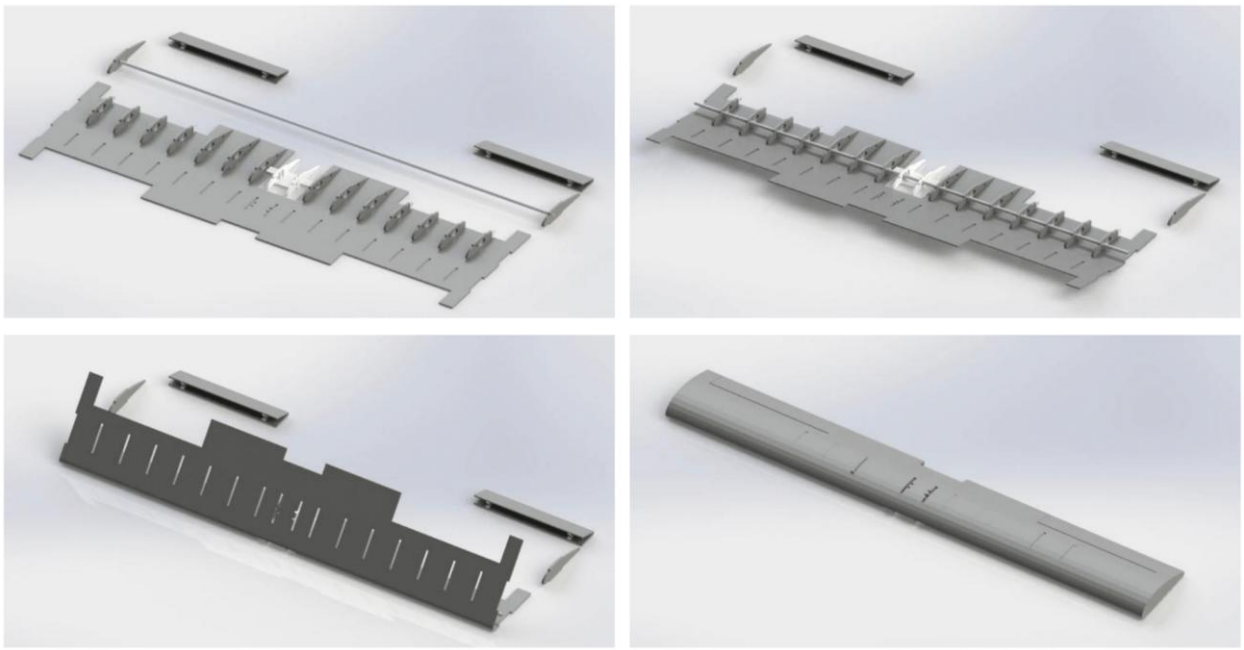

Figure 13. Wing folding process

2.3.2. Movable wing system for payload adaptability

The center of gravity (CG) position is crucial for an aircraft's pitch stability and control. A forward CG creates a greater degree of stability, but increased control effort and power are required, while an aft CG leads to instability, making pitch control challenging [9]. In order to achieve stable flight under various mission scenarios, EAVDAR uses a movable wing system for fine-tuning the dynamics according to the varying distribution of payload. Figure 13 shows the wing's configurability to adapt to varying payload requirements. This adaptability allows the UAV to remain stable during autonomous operation but be sufficiently agile for precise navigation.

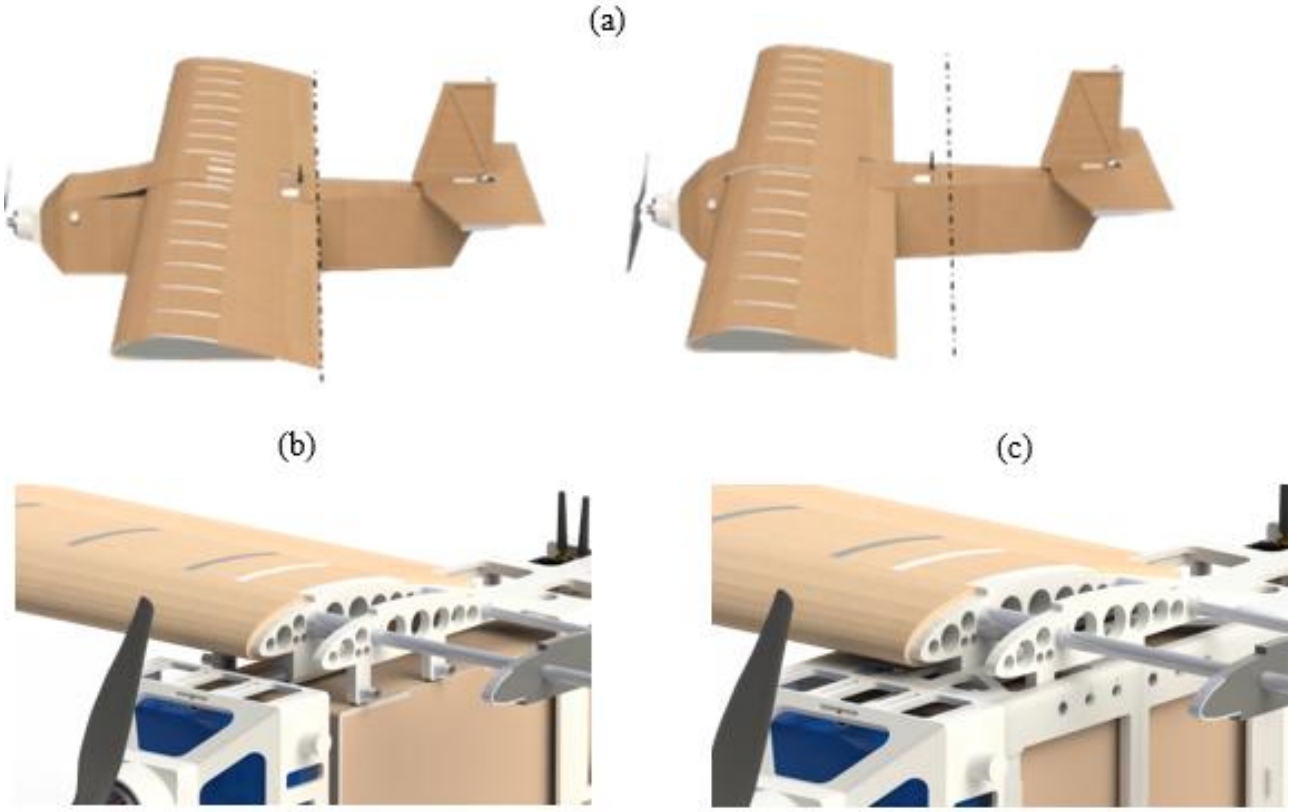

Figure 14. Movable wing for variable payloads: (a) different wing position configuration; (b) internal wing hub mechanism; (c) internal hub to body locking

EAVDAR's high-wing configuration further enhances stability by creating a pendulum effect, where the weight of the fuselage below the wing helps to eliminate roll disturbances. The modified airfoil, designed with respect to the NACA 4415 airfoil, was chosen due to its high lift performance at low speed, higher aerodynamic efficiency, and steady flight behavior [10]. The placement of the wing and tailplane was optimized with regard to keeping the CG within 5-15% of the mean aerodynamic chord, thus allowing for a stable static margin without requiring an excessive nose-weight [11].

3. Aerodynamic performance

3.1. Computational aerodynamic analysis of EAVDAR

The aerodynamic performance of the EAVDAR UAV was evaluated utilizing the Digital DATCOM, XFLR5, and SolidWorks CFD to assess the efficiency, stability, and overall flight characteristics. These computational tools allowed a multilevel assessment in which lifting forces, drag, stability margins, and pressure distributions could be addressed in order to optimize the aerodynamics of the UAV for the mission type to be accomplished [13].

3.1.1. Digital DATCOM

Digital DATCOM was utilized for preliminary aerodynamic studies using a blend of theory and empirical methods to ascertain lift, drag, and pitching moment numbers. This utility performed quick calculations, which formed the base for aerodynamic performance analysis of the UAV, and iterative design upgrades guided by the lift-to-drag ratio and stability requirement. DATCOM's predictions supported the development of the early airframe configuration by providing information on maximum lift coefficient, aerodynamic efficiency, and effectiveness of control surfaces, all of which were required to deliver stable and efficient flight of the UAV.

```
CASEID for005.dat
 $FLTCON NALPHA=20.0,ALSCHD=-9.0,-8.0,-7.0,-6.0,-5.0,-4.0,-3.0,-2.0,-1.0,0.0,
  1.0,2.0,3.0,4.0,5.0,6.0,7.0,8.0,9.0,10.0,
  NALT=1.0,ALT=100.0,
  NMACH=1.0,MACH=0.058,
  WT=15.40,LOOP=2.0$
 $OPTINS SREF=8.53,CBARR=1.30,BLREF=6.56$
 $SYNTHS XCG=0.94,ZCG=0.00,XW=0.50,ZW=0.30,ALIW=5.70,
  XH=3.00,ZH=0.32,ALIH=0.00,XV=3.00,YV=0.00,ZV=0.29,VERTUP=.TRUE.$
 $BODY NX=6.0,ITYPE=1.0,
  X=0.05,0.06,0.29,1.62,3.29,3.59,
  ZU=-0.00,0.07,0.27,0.29,0.27,0.28,
  ZL=-0.00,-0.07,-0.30,-0.31,-0.30,0.22,
  R=0.00,0.14,0.29,0.29,0.09,0.06,
  P=5.00,5.00,5.00,5.00,5.00,5.00,
  S=0.000,0.063,0.261,0.267,0.027,0.012,$
NACA-W-4-4712
 $WGPLNF CHRDR=1.30,CHRDBP=1.30,CHRDTP=1.30,SSPN=3.28,
  SSPNE=3.43,SSPNOP=0.00,SAVSI=0.00,SAVSO=0.00,
  CHSTAT=0.25,DHDADI=0.00,DHDADO=0.00,TYPE=1.0$
NACA-H-4-0006
 $HTPLNF CHRDR=0.59,CHRDBP=0.59,CHRDTP=0.36,SSPN=1.15,
  SSPNE=0.98,SSPNOP=0.00,SAVSI=0.00,SAVSO=0.00,
  CHSTAT=1.00,DHDADI=0.00,DHDADO=0.00,TYPE=1.0$
NACA-V-4-0012
 $VTPLNF CHRDR=0.59,CHRDBP=0.59,CHRDTP=0.36,SSPN=0.79,
  SSPNE=0.62,SSPNOP=0.69,SAVSI=0.00,SAVSO=0.00,
  CHSTAT=1.00,DHDADI=0.00,DHDADO=0.00,TYPE=1.0$
 $SYMFLP SPANFI=0.306,SPANFO=0.917,CHRDFI=0.306,CHRDFO=0.306,
  FTYPE=1.000,PHETE=0.003,PHETEP=0.002,TC=0.220,CB=0.300,
  NDELTA=1.0,DELTA=0.0,$
 $ASYFLP SPANFI=0.917,SPANFO=3.280,CHRDFI=0.153,CHRDFO=0.153,
  STYPE=1.000,NDELTA=1.0,
  DELTAL=0.0,
  DELTAR=0.0,$
 $SYMFLP SPANFI=0.306,SPANFO=1.150,CHRDFI=0.153,CHRDFO=0.153,
  FTYPE=1.000,PHETE=0.003,PHETEP=0.002,TC=0.220,CB=0.300,
  NDELTA=1.0,DELTA=0.0,$
PLOT
NEXT CASE
```

Figure 15. Input file for Digital DATCOM aerodynamic analysis of the EAVDAR UAV

Figure 14 shows the input text file for the Digital DATCOM analysis of EAVDAR, which is produced using the Aircraft Intuitive Design (AID) [12] application. The file includes aerodynamic data and geometry files required for stability and control calculations. In the case of Digital DATCOM analysis, the main wing is modeled using the NACA 4712 airfoil as depicted in Figure 15. The airfoil is turned 5.7 degrees to properly approximate the original wing configuration. Both the horizontal and vertical tail surfaces assume the NACA 0006 airfoil, and they are considered as thin, flat plates in order to model their stabilizing effect. In addition, the CG is located 130 mm behind the leading edge, which can be considered a key point in analyzing the stability and control performances of the UAV.

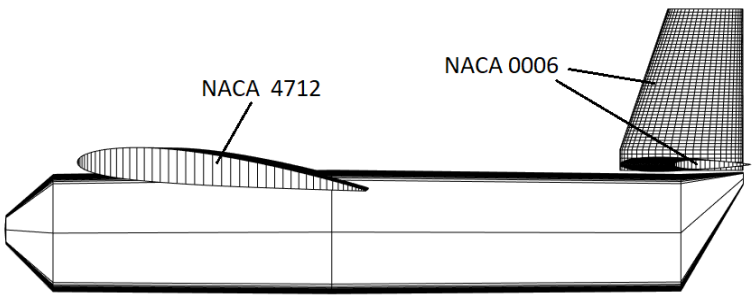

Figure 16. Approximation of the EAVDAR wing and tail surfaces in digital DATCOM

3.1.2. XFLR5

To further refine the aerodynamic model, XFLR5 was employed to analyze the UAV's low-speed aerodynamic behavior—an essential aspect for achieving sustained flight and controlled landings, particularly in humanitarian and reconnaissance missions. Utilizing panel methods and vortex lattice techniques [13], XFLR5 provided detailed insights into wing aerodynamics, flow separation, and stability derivatives, which informed the optimization of the UAV's wing and control surface configurations for improved endurance and maneuverability. The tool enabled the evaluation of key aerodynamic characteristics, including lift distribution, flow behavior, and stability responses.

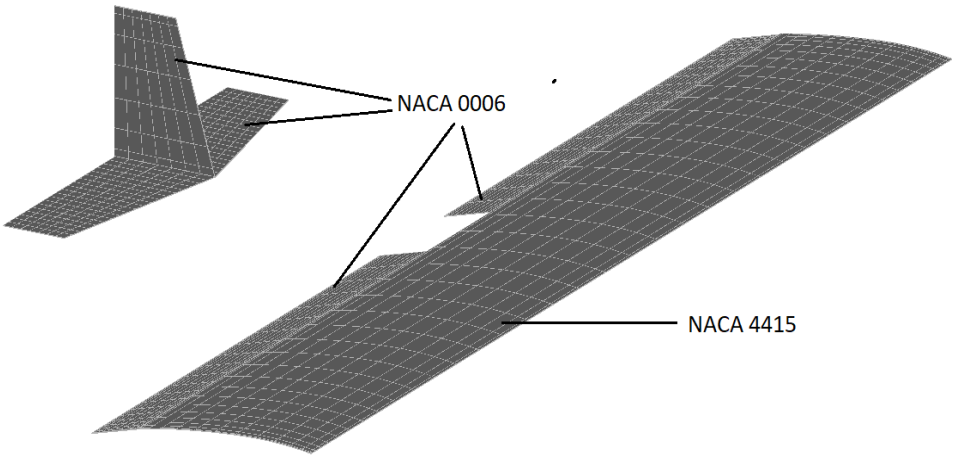

Figure 17. XFLR5 model for the aerodynamic analysis of EAVDAR

Figure 16 presents the XFLR5 model of the EAVDAR UAV, emphasizing the wing and empennage configuration. The fuselage is excluded, as XFLR5 primarily focuses on the analysis of lifting surfaces. For this analysis, a more detailed representation of the wing geometry was implemented. As shown in the figure, the main wing was divided into two sections: the primary lifting surface utilized the NACA 4415 airfoil, while the trailing edge and aileron region were modeled using the NACA 0006 airfoil to better approximate the thin control surfaces. The horizontal and vertical stabilizers also employed the NACA 0006 profile, consistent with the DATCOM configuration. To maintain consistency in stability and control evaluations between both analyses, the center of gravity was set at 130 mm from the leading edge of the wing.

3.1.3. SolidWorks CFD

To evaluate the aerodynamic efficiency in more detail and a pragmatic manner, SolidWorks Flow Simulation was used to perform computational fluid dynamics (CFD) analyses. This method allowed airflow phenomena, pressure distributions, and potential sources of drag along the UAV's fuselage and wings to be studied with greater detail. The simulations pinpointed regions of unfavorable pressure gradients and flow separation, which guided improvements in the aerodynamic shaping, resulting in lower drag and better overall flight performance.

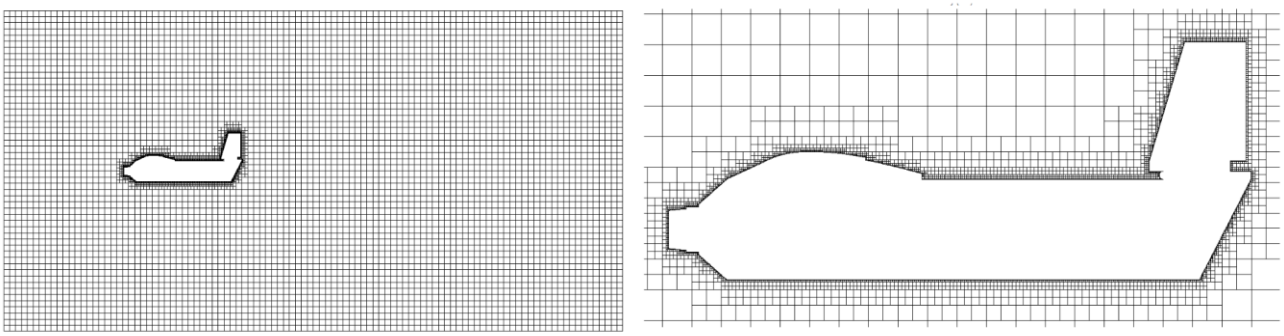

Figure 18. 2D view of the computational mesh used in SolidWorks CFD, consisting of 2 $\times 10^6$ cells

The computational grid used in the CFD simulation, with approximately 2×10^6 cells, is shown in Figure 17. The mesh is locally refined around the UAV, especially around the fuselage, wing, and empennage, to achieve the correct resolution of the flow structures. This perturbation accounts for crucial aerodynamic features—including boundary layer growth, flow separation, and pressure gradients—that are required for reliable prediction of performance. The integration of SolidWorks Flow Simulation offers a more realistic representation of the UAV's aerodynamic behavior, complementing the lower-fidelity models employed in earlier design phases. By leveraging CFD, the study deepens the understanding of aerodynamic performance, supporting both design optimization and performance validation.

3.2. Performance metrics

The aerodynamic performance of the UAV was evaluated using key metrics obtained from DATCOM, XFLR5, and SolidWorks CFD. Figure 18 presents the coefficient of lift as a function of the angle of attack, assessed at 20 m/s (Re ≈ 400,000). Within the flight range of α (-9° to +5°), DATCOM and XFLR5 yield nearly identical results, suggesting a strong correlation between the two methods. The curve approximates a straight line, with its slope—known as Cl_α—being a critical aerodynamic coefficient. Both DATCOM and XFLR5 predict a Clα of approximately 5.7, while SolidWorks CFD estimates a slightly higher value of 5.9, likely due to its more detailed modeling of three-dimensional and viscous effects. The zero-lift angle of attack is approximately -9° according to both DATCOM and XFLR5, while SolidWorks CFD predicts -8°, which indicates a slight deviation due to different model principles. The lift coefficient at zero α is 0.89 for DATCOM and XFLR5, whereas SolidWorks CFD predicts 0.81, indicating a marginal loss in lift in the CFD model, likely due to improved boundary layer treatment effects. Overall, the agreement of the three methods in this angle of attack range among themselves confirms the validity of the aerodynamic predictions and the confidence in the UAV lift behavior.

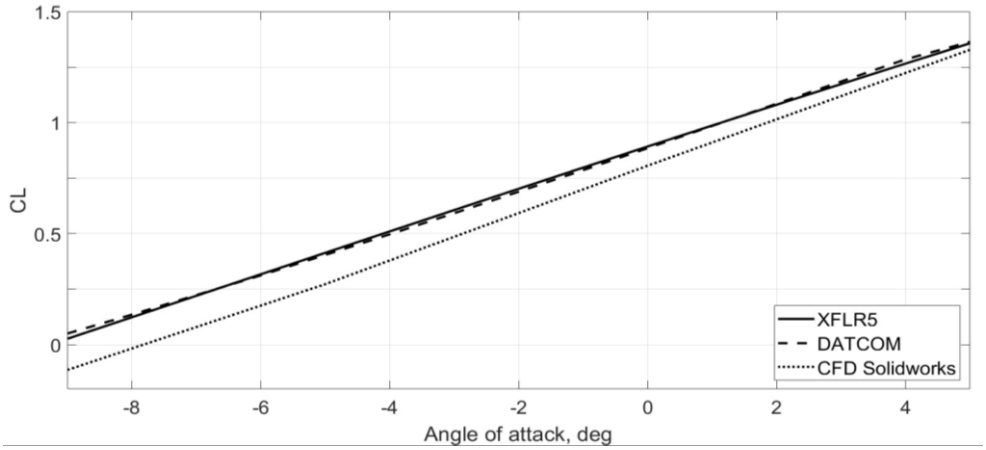

Figure 19. Coefficient of lift vs angle of attack

The aerodynamic performance of the UAV is characterized by its drag polar, the relationship between the coefficient of lift, Cl, and the coefficient of drag, Cd. This relationship is of particular importance for determining the optimal lift-to-drag ratio (Cl/Cd) if the effect of induced velocity on endurance and other flight properties is to be evaluated. A higher Cl/Cd ratio indicates lower drag at the same amount of lift, and hence increases energy efficiency and flight distance for the UAV.

In order to make a fair comparison on aerodynamic efficiency, the minimum drag coefficient (Cd) values from XFLR5 and DATCOM were modified to align with the value predicted by SolidWorks CFD. This correction is necessitated by intrinsic shortcomings of the lower-fidelity tools: XFLR5 does not consider the drag of the fuselage and hence would underestimate the total drag, and DATCOM generally underestimates the drag at low Reynolds numbers that are characteristic of the flight of UAVs. By calibrating the low-fidelity Cd values against the higher-fidelity CFD results, a more accurate and consistent modeling of the UAV's aerodynamic performance is obtained.

The drag polar from XFLR5, DATCOM, and SolidWorks CFD is shown in Figure 19. The results from XFLR5 and DATCOM are closely aligned, predicting a maximum Cl/Cd of 7.8. The CFD analysis, which includes fuselage and 3-D flow effects, however, predicts a significantly greater maximum Cl/Cd of 8.5. It indicates that lower-fidelity methods may overestimate induced drag while underrepresenting the effects from the contributions of the fuselage to overall aerodynamic loadings. The higher efficiency observed in CFD results implies that fuselage shaping and interaction effects of the flow are more important than initially aeroelastic models depicted, emphasizing the need for more fidelity analysis to refine UAV design.

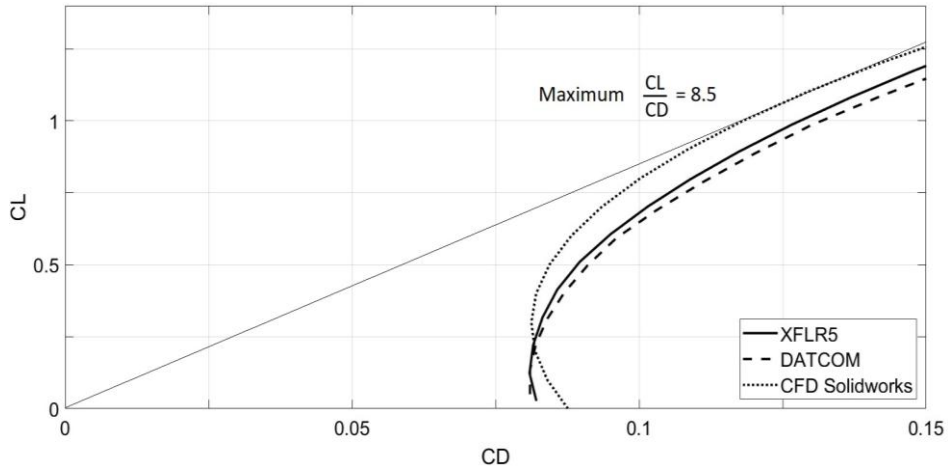

Figure 20. Drag polar; Minimum drag coefficient in XFLR5 and DATCOM adjusted to match CFD results

These results demonstrate the inadequacy of panel methods to properly model three-dimensional drag components, thus calling for computational fluid dynamics (CFD) validation of the next design. Although XFLR5 and DATCOM yield rapid approximations that are handy for conceptual design, a comprehensive CFD analysis is still necessary in order to maximize aerodynamic efficiency and enable reliable predictions of performance.

3.3. Stability analysis

The stability of the EAVDAR UAV was evaluated using static stability criteria (SSC), which is necessary for ensuring reliable operation under different flight conditions [14]. The SSC and the corresponding values for EAVDAR can also be compared from Table 5. The aerodynamic coefficients and stability derivatives were obtained exclusively through XFLR5 stability analysis, which offers a simple route for determining all parameters automatically. A UAV mass of 7 kg was used for the analysis, corresponding to a trim flight velocity of 15 m/s. The results offer a comprehensive assessment of the UAV's static stability properties, validating its capability to fly stably within its flight envelope.

The longitudinal stability analysis has demonstrated that the UAV meets the SSC #1, with a stabilizing nose-down moment when thrust changes take place. This characteristic is essential for maintaining controlled flight across various power settings. The positive lift curve slope ($cL\alpha$ = 5.48) indicates that lift increases proportionally with the angle of attack (AOA), while the negative pitching moment coefficient slope ($cm\alpha$ = -1.13) ensures that the pitching moment decreases with increasing AOA, thus reducing the risk of excessive nose-up characteristics leading to stall.

The UAV possesses satisfactory properties of lateral and directional stability. The negative side force coefficient slope ($cY\beta$ = -0.141) provides directional stability by generating a restoring yaw force to sideslip. As a result, the positive yawing moment coefficient slope ($cn\beta$ = 0.051) produces a stabilizing effect in the yawing moment sense. Roll damping is clearly demonstrated by the negative roll damping coefficient (clp = -0.533), which effectively dissipates roll oscillations and contributes to better operation in banked turns or in a turbulent atmosphere.

Table 5. Static stability criteria for EAVDAR

Stability Criteria		EAVDAR	Remarks
SSC #1	$c_{TXu} - c_{Du} < 0$	$c_{TXu} = -0.16$, $c_{Du} = 0$	Stable
SSC #2	$c_{Y\beta} < 0$	$c_{Y\beta} = -0.141$	Stable
SSC #3	$c_{L\alpha} > 0$	$c_{L\alpha} = 5.48$	Stable
SSC #4	$c_{m\alpha} < 0$	$c_{m\alpha} = -1.13$	Stable
SSC #5	$c_{n\beta} > 0$	$c_{n\beta} = 0.051$	Stable
SSC #6	$c_{lp} < 0$	$c_{lp} = -0.533$	Stable
SSC #7	$c_{mq} < 0$	$c_{mq} = -7.60$	Stable
SSC #8	$c_{nr} < 0$	$c_{nr} = -0.034$	Stable
SSC #9	$c_{l\beta} < 0$	$c_{l\beta} = -0.009$	Stable
SSC #10	$c_{mu} > 0$	$c_{mu} = -0.011$	Unstable

The aircraft's damping characteristics further support stable flight. The negative pitch damping coefficient ($c_{mq} = -7.6$) and yaw damping coefficient ($c_{nr} = -0.034$) ensure suppression of oscillatory behavior, leading to smooth attitude recovery following perturbations. Additionally, the negative rolling moment coefficient due to sideslip ($c_{l\beta} = -0.009$) stabilizes roll behavior during sideslip conditions, preventing excessive lateral deviations.

The UAV demonstrates strong static stability across most criteria, ensuring predictable and controlled flight characteristics. However, the slightly negative speed stability derivative ($c_{mu} = -0.011$) suggests a potential sensitivity to rapid speed changes. A negative CMU value indicates that an increase in velocity may induce a slight nose-down pitching moment, which could lead to minor oscillations in pitch stability. While this is not a very destabilizing phenomenon, it has the effect of diminishing the UAV's natural pitch-trim tendency after sudden changes in velocity. This type of behavior needs to be investigated further, especially at times of high acceleration or sudden throttle changes. Possible solutions involve changing the longitudinal static margin or optimizing control system gains to increase pitch responsiveness and smooth transition during changes in speed.

4. Structural analysis

To complement the aerodynamic performance assessment, a detailed wing structural analysis was performed to evaluate the drone's ability to withstand operational loads under varying flight conditions. Methodologies from previous studies were followed for this analysis [15-17]. Aerodynamic surface pressure distributions were generated using CFD simulations for a range of AOA spanning from –10° to +15°. These pressures were then applied as boundary conditions in a finite element model using ANSYS Static Structural to assess stress distribution and deformation for the wing assembly. This approach ensures that the airframe design maintains sufficient structural integrity and durability while adhering to the low-cost, readily manufacturable system of EAVDAR.

The skin material of EAVDAR was modeled as sintraboard; however, only the bulk material properties of the foam core [18] are considered in the structural analysis. The drone assembly includes aluminum rods made from 6061-T6 alloy, and the 3D-printed parts are modeled using PLA material. Table 6 highlights the material properties applied for this analysis. Table 7 summarizes the wing structural response under aerodynamic loading for AOA from –10° to +15°. The results show the maximum deformation and equivalent stress for the sintraboard, aluminum rods, and PLA components, as well as the corresponding factor of safety for each material. The highest recorded maximum deformation occurs at +5° AOA.

Table 6. EAVDAR wing structural response

AOA	Maximum Deformation, mm	Sintraboard			Aluminum Rods			PLA Structures		
		Maximum Stress, MPa	Material Yield Stress, MPa [18]	Factor of Safety	Maximum Stress, MPa	Material Yield Stress, MPa [20]	Factor of Safety	Maximum Stress, MPa	Material Yield Stress, MPa [19]	Factor of Safety
-10°	30.781	0.056	0.9	16.07	12.361	265	21.44	0.7527	31.8	42.25
-5°	72.125	0.1312	0.9	6.86	28.964	265	9.15	1.7637	31.8	18.03
0°	168.41	0.3063	0.9	2.94	67.631	265	3.92	4.1182	31.8	7.72
5°	244.35	0.4445	0.9	2.02	98.124	265	2.70	5.975	31.8	5.32
10°	207.9	0.3782	0.9	2.38	83.490	265	3.17	5.0839	31.8	6.26
15°	216.7	0.3942	0.9	2.28	87.022	265	3.05	5.299	31.8	6.00

For the sintraboard, equivalent stress values increase with AOA from 0.056 MPa at –10° to a maximum of 0.4445 MPa at +5°. The aluminum rods show the highest equivalent stress overall, rising from 12.361 MPa at –10° to a maximum of 98.124 MPa at +5°. The PLA parts follow a similar trend, with stresses ranging from 0.7527 MPa at –10° up to 5.975 MPa at +5°. Moreover, the safety factor of the design materials printed in EAVDAR displayed reasonable margins for all flight operating conditions. This implies that the structure can reliably withstand aerodynamic loads without the possibility of premature failure. The total wing deformation and stress distribution at an AOA of +5° are presented in Figure 21.

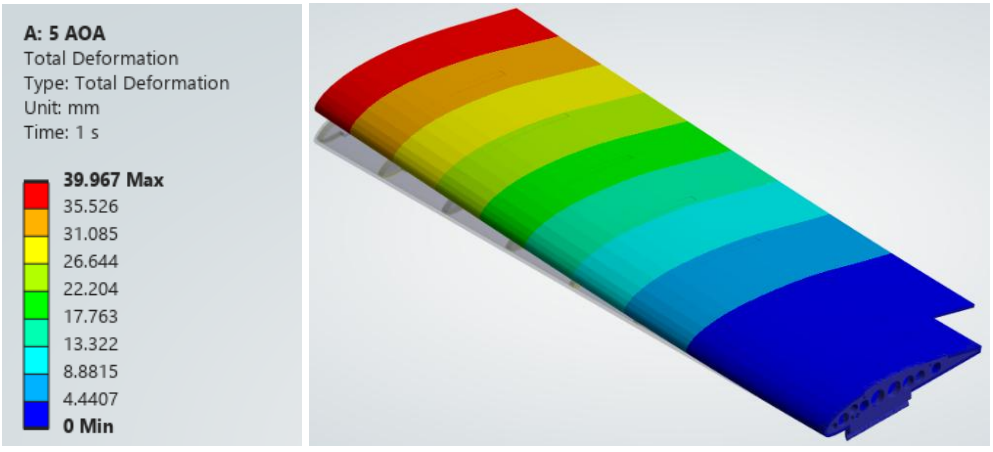

(a)

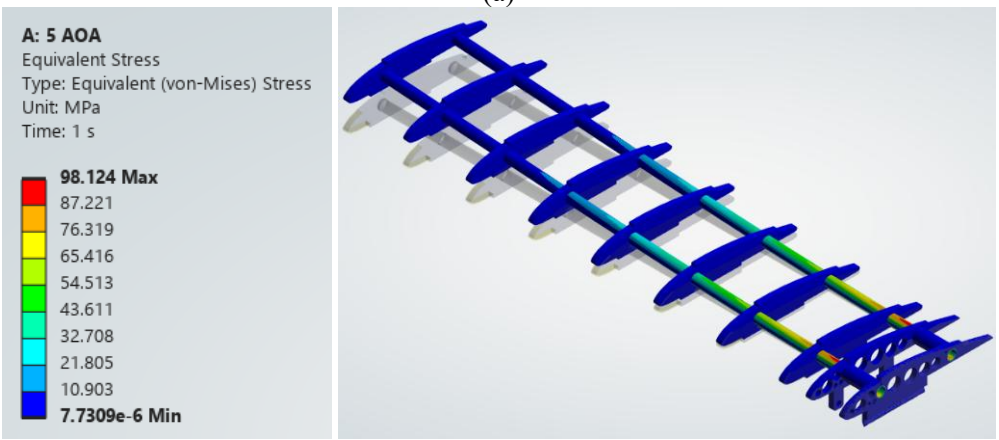

(b)

Figure 21. (a) EAVDAR Total Wing Deformation, and (b) Wing Stress Distribution (Bottom) at +5° AOA

Throughout the tested range, the sintraboard material, aluminum rods, and PLA components all show stress levels and deflection patterns consistent with their intended structural roles within the airframe. Overall, the findings confirm that the combination of readily available materials and simple structural design can provide sufficient load-bearing capacity and durability for the intended low-cost, expendable UAV application. This analysis also highlights areas where local reinforcement or material selection adjustments may be considered to maintain structural reliability across diverse operating scenarios.

5. Flight simulation using XPlane

The flight dynamics and waypoint-tracking performance of EAVDAR were evaluated using a configuration-matched model in X-Plane 12 that reproduced the airframe geometry, mass properties, and autopilot tuning. Steady winds were applied from the north, east, south, and west at 15, 20, and 25 knots to represent post-disaster operating conditions in which typhoon-level winds are not expected. Across all wind directions and speeds (see Figures 23–25), the UAV maintained stable autonomous flight and consistently reached its waypoints with acceptable accuracy. Under 15-knot winds, the mean position error was approximately 1–3 m. In the most demanding case—a 25-knot crosswind—short, meter-scale lateral offsets occurred during waypoint transitions but were rapidly corrected by the autopilot, with mean waypoint error remaining approximately 10–11 m. Headwinds reduced throttle demand, whereas tailwinds modestly increased control effort during low-altitude turns. These outcomes indicate adequate control authority and navigation robustness within the intended operating envelope. The simulator's flight-dynamics engine has been validated against real-world data with greater than 92% agreement on key dynamic metrics [20], supporting the use of these trials as a rigorous pre-prototype performance screen.

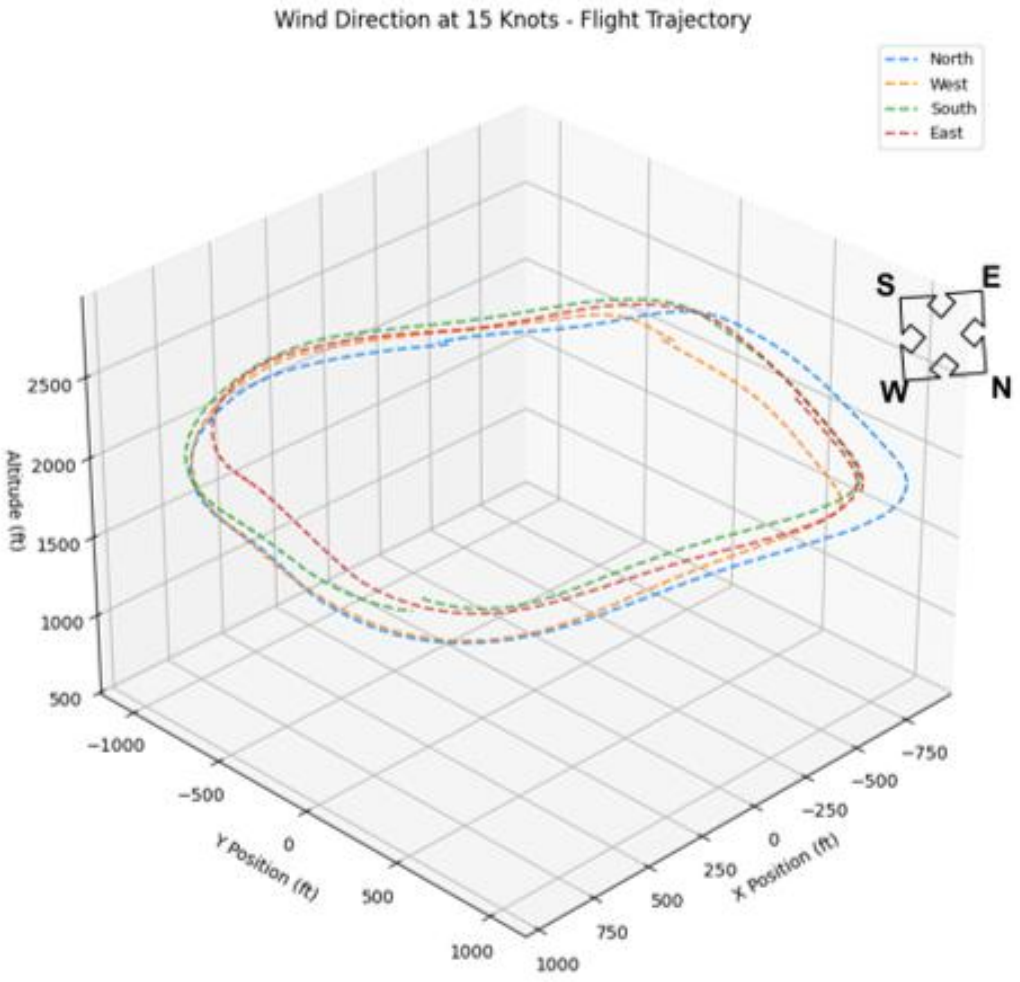

Figure 22. Flight trajectory on different wind directions at 15 knots

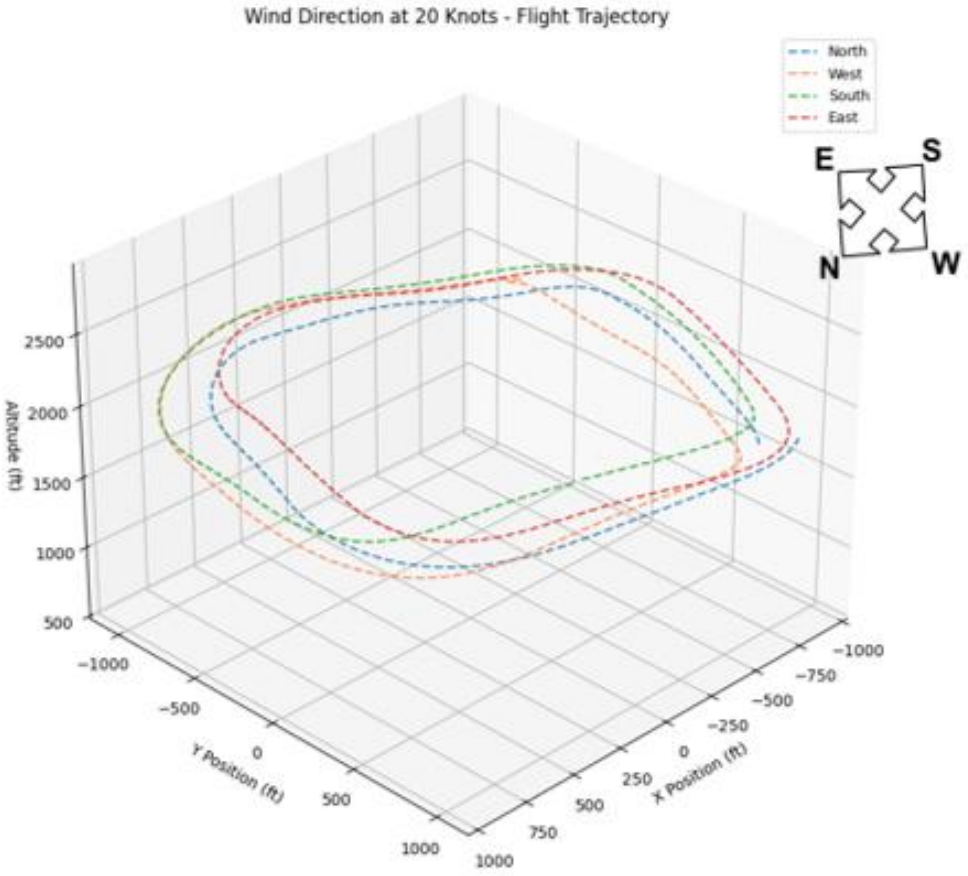

Figure 23. Flight trajectory on different wind directions at 20 knots

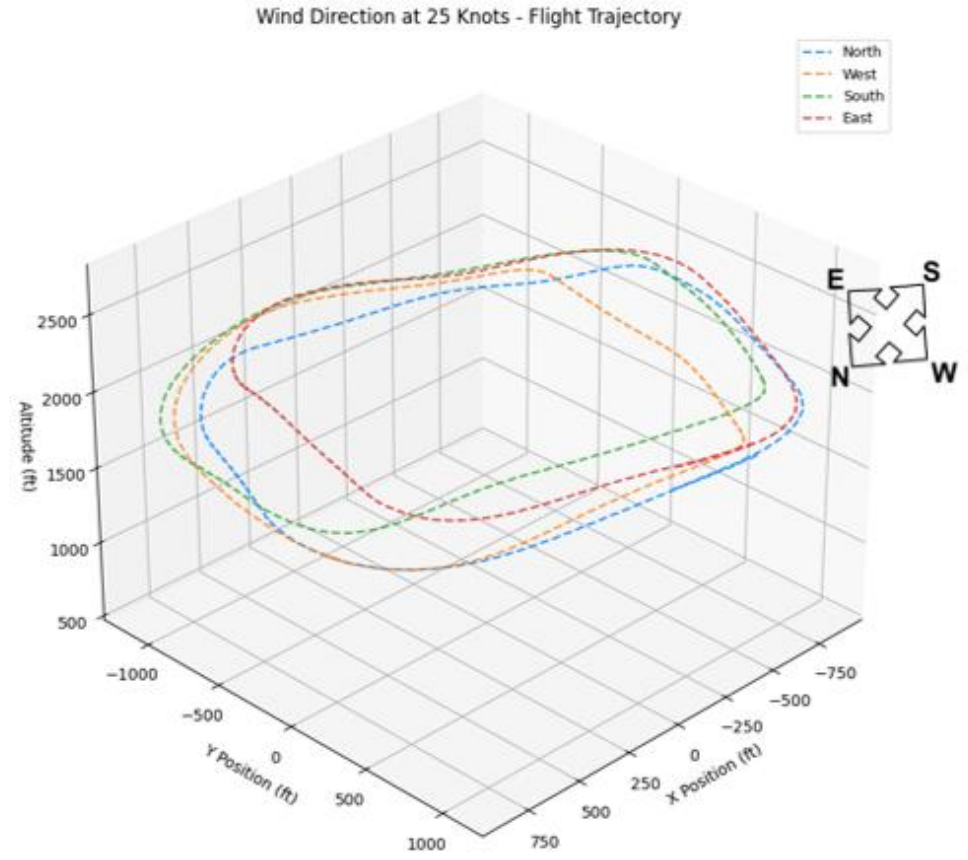

Figure 24. Flight trajectory on different wind directions at 25 knots

6. Conclusions

This study successfully designed and evaluated a low-cost, expendable fixed-wing drone for humanitarian applications using off-the-shelf components. Computational analyses verify its stable flight, with efficient aerodynamics and cost effectiveness in disaster relief and humanitarian applications.

The optimized wing and fuselage enable an increased lift-to-drag ratio, thereby increasing endurance and reliability. Using commercially available components ensures affordability and scalability, while the modular design allows it to be reconfigured for a multitude of different payloads.

Furthermore, the structural analysis conducted using CFD-derived pressure loading in ANSYS demonstrates that the drone's wing responds predictably to aerodynamic forces across a representative range of flight conditions. Most importantly, the simulations show that using off-the-shelf components for EAVDAR provides sufficient structural strength and integrity for its role as a low-cost, expendable UAV.

Future work will involve integrating a vision-based survivor detection system that will enhance search-and-rescue capabilities, and real-world field testing will validate performance across diverse conditions.

This study advances cost-effective UAV solutions for humanitarian aid, bridging the gap between affordability and performance.

Declaration of competing interest

All authors declared no known financial or non-financial competing interests in any material discussed in this paper.

Funding information

Funding was received from Mindanao State University - Iligan Institute of Technology (MSU-IIT) and Department of Science and Technology-Engineering Research and Development for Technology (DOST-ERDT).

Acknowledgements

The Robotics, Instrumentation, and Control Engineering Laboratory extends our sincere gratitude to Mindanao State University - Iligan Institute of Technology (MSU-IIT) for their support in providing the foundation for this research. We also thank the Engineering Research and Development for Technology (ERDT) for the scholarship funding that supported this project, and the Department of Mechanical Engineering and Technology (DMET) of MSU-IIT for providing the tools and equipment necessary to conduct this research.

Author contribution

The contribution to the paper is as follows: Michael Ray Maligro: Lead researcher; Donato Juayang Jr.: study conception, design, and analysis; Alan Pierre-Miguel Gultia, Paula Alexandra Padro, Ben James Cuajotor, Michael Caleb Obalan, Dynah Ruiza Opeso, Kristy Lailanie Ompad: data collection and drone development; Sherwin Guirnaldo is the principal researcher; Noel Hernandez, Jonathan Maglasang: research advisement and consultants. All authors approved the final version of the manuscript.

References

[1] M. Lyu, Y. Zhao, C. Huang, and H. Huang, "Unmanned aerial vehicles for search and rescue: A survey," *Remote Sensing*, vol. 15, no. 13, p. 3266, 2023.

[2] C. M. G. Villame and S. Guirnaldo, "Design and implementation of a voice-command controller for fixed-wing unmanned aerial vehicles using automatic speech recognition and natural language processing techniques," *Sustainable Engineering and Innovation*, vol. 6, no. 2, pp. 199–212, 2024.

[3] F. Sattar, L. Tamatea, and M. Nawaz, "Droning the pedagogy: Future prospects of teaching and learning," *International Journal of Educational and Pedagogical Sciences*, vol. 11, no. 6, pp. 1650–1655, 2017.

[4] sUAS News, "SYPAQ and Tanglewood Group Partner for Global 'Corvo' PPDS UAS Delivery," *sUAS News*, Jun. 2023. [Online]. Available: https://www.suasnews.com/2023/06/sypaq-and-tanglewood-group-partner-for-global-corvo-ppds-uasdelivery/

[5] D. Pascarella *et al*., "A methodological framework for the risk assessment of drone intrusions in airports," *Aerospace*, vol. 9, no. 12, p. 747, 2022.

[6] M. Algan, M. Seyhan, and M. Sarioğlu, "Effect of aero-shaped vortex generators on NACA 4415 airfoil," *Ocean Engineering*, vol. 291, p. 116482, 2024. https://doi.org/10.1016/j.oceaneng.2023.116482

[7] M. El Adawy *et al*., "Design and fabrication of a fixed-wing Unmanned Aerial Vehicle (UAV)," *Ain Shams Engineering Journal*, vol. 14, no. 9, p. 102094, 2023.

[8] K. Chinwicharnam and C. Thipyopas, "Comparison of wing–propeller interaction in tractor and pusher configuration," *International Journal of Micro Air Vehicles*, vol. 8, no. 1, pp. 3–20, 2016.

[9] M. Voskuijl, "Performance analysis and design of loitering munitions: A comprehensive technical survey of recent developments," *Defence Technology*, vol. 18, no. 3, 2021. https://doi.org/10.1016/j.dt.2021.08.010

[10] Intergovernmental Panel on Climate Change, *Aviation and the Global Atmosphere: A Special Report of IPCC Working Groups I and III*. Cambridge University Press, 1999. https://www.grida.no/climate/ipcc/aviation/097.htm

[11] J. B. Russell, *Performance and Stability of Aircraft*. Oxford: Butterworth-Heinemann, 2003.

[12] B. W. McCormick, *Aerodynamics, Aeronautics, and Flight Mechanics*. John Wiley & Sons, 1994.

[13] M. Napolitano, *Aircraft Dynamics: From Modeling to Simulation*. Wiley Global Education, 2011.

[14] Z. Lietzau, *Aircraft Intuitive Design (AID)*, MATLAB Central File Exchange, 2025. https://www.mathworks.com/matlabcentral/fileexchange/66770-aircraft-intuitive-design-aid

[15] A. Nath, R. Anand, J. Desai, M. T. H. Sultan, and S. A. Raj, "Modelling and finite element analysis of an aircraft wing using composite laminates," *IOP Conference Series: Materials Science and Engineering*, vol. 1183, no. 1, p. 012006, Sep. 2021. https://doi.org/10.1088/1757-899x/1183/1/012006

[16] E. I. Basri *et al*., "UAV NACA4415 wing structural performance analysis subjected to external aerodynamic load using Schrenk's approximation," *Journal of Advanced Research in Fluid Mechanics and Thermal Sciences*, vol. 60, no. 2, pp. 178–190, Jan. 2019.

[17] K. K. Rumayshah, A. Prayoga, and M. A. Moelyadi, "Design of high altitude long endurance UAV: Structural analysis of composite wing using finite element method," *Journal of Physics: Conference Series*, vol. 1005, p. 012025, Apr. 2018. https://doi.org/10.1088/1742-6596/1005/1/012025

[18] C. Uzay, N. Geren, M. Boztepe, and M. Bayramoglu, "Bending behavior of sandwich structures with different fiber facing types and extremely low-density foam cores," *SSRN Electronic Journal*, Jan. 2019. https://doi.org/10.2139/ssrn.3421868

[19] F. Franke, U. Burger, and C. Hühne, "A novel reduced order model for drone impacts with aircraft structures," *CEAS Aeronautical Journal*, vol. 14, no. 2, pp. 381–412, Feb. 2023. https://doi.org/10.1007/s13272-023-00646-1

[20] M.-H. Do, C.-E. Lin, and Y.-C. Lai, "Validation of the flight dynamics engine of the X-Plane simulator in comparison with the real flight data of the quadrotor UAV using CIFER," *Drones*, vol. 7, no. 9, p. 548, 2023.